Meshing Meristems - An Iterative Mesh Optimization Method for Modeling Plant Tissue at Cell Resolution

Guillaume Cerutti, Christophe Godin

Meshing Meristems
An Iterative Mesh Optimization Method for Modeling Plant Tissue at Cell Resolution

Guillaume Cerutti and Christophe Godin
INRIA, Virtual Plants INRIA Team, Montpellier, France
{guillaume.cerutti, christophe.goding@inria.fr

Keywords: Mesh Optimization, Shoot Apical Meristem, Deformable Models, Cell Reconstruction, Morphogenesis.

Abstract: We address in this paper the problem of reconstructing a mesh representation of plant cells in a complex, multi-layered tissue structure, based on segmented images obtained from confocal microscopy of shoot apical meristem of model plant *Arabidopsis thaliana*. The construction of such mesh structures for plant tissues is currently a missing step in the existing image analysis pipelines. We propose a method for optimizing the surface triangular meshes representing the tissue simultaneously along several criteria, based on an initial low-quality mesh. The mesh geometry is deformed by iteratively minimizing an energy functional defined over this discrete surface representation. This optimization results in a light discrete representation of the cell surfaces that enables fast visualization, and quantitative analysis, and gives way to *in silico* physical and mechanical simulations on real-world data. We provide a framework for evaluating the quality of the cell tissue reconstruction, that underlines the ability of our method to fit multiple optimization criteria.

1 INTRODUCTION

The spectacular development of 3-dimensional microscopy imaging techniques over the past few years has opened a brand new field of experimental investigation for developmental biology. The huge amounts of data produced require the development of complete software pipelines to process automatically the image sequences capturing the living tissues. The automatic segmentation of cells and the tracking of cell lineages over time allows to quantify tissue growth, cell deformation and gene expression patterns.

However, segmented images constitute massive objects, and lighter and more versatile data structures that represent the shape of the cells are preferable to the raw voxel information. Triangular meshes are a compressed representation that make visualization easier and various computations on surfaces and volumes much more efficient. It is also a necessary object for a great deal of physical simulations, notably those based on finite elements methods. We consider then the problem of converting a 3-dimensional image stack of segmented cell tissue into a triangular mesh representing the surfaces the cells.

Our work is focused on images of shoot apical meristems (SAM) of *Arabidopsis thaliana* acquired by confocal laser scanning microscopy (CLSM) such as the one shown in Figure 1, and segmented using the MARS software pipeline (Fernandez et al., 2010). SAMs constitute small niches of dividing cells where all the aerial organs of a plant (inflorescence, leaves or branches), originate from. The study of sequences of cell tissue on the SAM is therefore a key step for a better understanding of morphogenesis in plants, and the growth of organs over time. The identification of cells, the reconstruction of their lineages and extraction of shape and semantic features at a cellular level are necessary steps in this analysis process.

In this context, we propose a tool to reconstruct

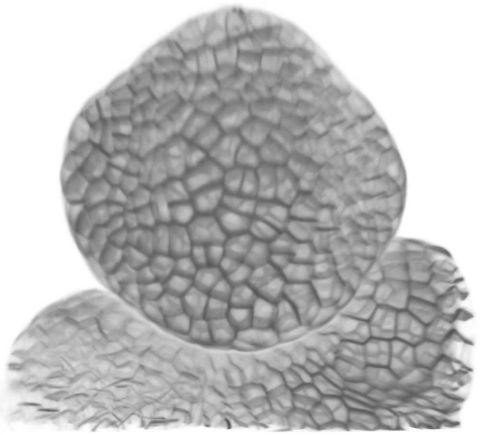

Figure 1: Confocal laser scanning image of an inflorescence meristem of *Arabidopsis thaliana*.

automatically the whole 3-D structure of a SAM by a discrete representation of cell surfaces. This mesh transforms the voluminous complex images into simple 3-D primitives, and includes topological relationships between cells as well as the estimation of their shape. In the following, we will present related work in Section 2. The generation of meshes is presented in Section 3 as well as the evaluation criteria we introduce, and the subsequent mesh optimization process is described in Section 4. Section 5 proposes an analysis of the results, as Section 6 draws conclusions and potential applications.

2 RELATED WORKS

The recent progresses in microscopy imaging make it possible to record the development of living tissues and organisms, with a temporal frequency that offers the novel opportunity of monitoring and modelling the processes at work at cell level (Keller, 2013).

2.1 Cell-scale Tissue Reconstruction

The interest of cell-scale tissue imaging for developmental biology is tremendous, and many works aim at building a digital reconstruction of living cells, considering different subjects of study : capturing the dynamics of plant shoot apical meristems (Fernandez et al., 2010; Tataw et al., 2013; Chakraborty et al., 2013) or following animal embryos during different development stages (Robin et al., 2011; Rizzi and Peyrieras, 2014; Guignard et al., 2014; Michelin et al., 2014).

Concerning the development of SAM cells (mostly of *Arabidopsis thaliana*) the works initially focused on the reconstruction of the surface (Kwiatkowska, 2004) to analyse the growth and division dynamics of the first layer of cells (L1) in the meristem (Barbier de Reuille et al., 2005). More recently, complete reconstructions of the dynamic multi-layered tissue structure have emerged, based on CLSM images, using a watershed segmentation algorithm (Fernandez et al., 2010) or representing cells as truncated ellipsoids (Chakraborty et al., 2011).

In contrast with pure image segmentation where the output is an image of labeled voxels, some methods provide a more discrete cell reconstruction, under the form of a Voronoi-like anisotropic tessellation (Chakraborty et al., 2013) or with tools allowing the definition of a triangular mesh on the surface of the meristem (Barbier de Reuille et al., 2014). Such a compact tissue reconstruction is a desirable output for fast quantification of cell properties, interactive visualization of large objects and models of tissue growth.

2.2 Mesh Generation and Optimization

A triangular mesh constitutes a discretization of a surface or a volume, and a generally more compressed view of an object, making it easier to manipulate. Different approaches have emerged to generate a mesh from a 3-dimensional image, most commonly using Marching Cubes (Lorensen and Cline, 1987) to produce a very high resolution mesh of the surfaces, or based on triangulated sample points (Shewchuk, 1998) to represent a volume by tetrahedra.

A common problem with mesh generation methods is the lack of control on the quality of the produced mesh. To obtain a satisfying result, some optimization is generally needed, either on the connectivity of the mesh elements (through local collapse or split operations (Hoppe et al., 1993)) or on their shape (Owen, 1998).

To improve the shapes of the mesh elements, a common approach is to smooth the mesh by adjusting the positions of its vertices. The most widespread method is the Laplacian smoothing (Field, 1988), where vertices are attracted by the barycenters of their neighbors, and that has been used widely in other mesh smoothing techniques (Freitag, 1997).

Another method is to consider smoothing as an optimization problem, where the quality of the mesh can be estimated locally, and the location of any point updated to improve the quality of its surroundings (Amenta et al., 1997; Freitag, 1997). In that case, the problem can be formulated as the minimization of an energy functional (Hoppe et al., 1993; Vidal et al., 2012), a framework that can also be used for segmentation and tracking purposes (Dufour et al., 2011). Such approaches allow a precise definition of the properties that should be optimized by the smoothing, as well as the inclusion of external constraints introducing some prior knowledge, and are well suited for domain-specific applications such as ours.

3 GENERATING TISSUE MESH

The first step towards the reconstruction of a mesh representation of a cell tissue is the generation of its topology. This implies that all the cells in the multilayered structure have to be identified to make the definition of interfaces between cells possible. Based on a confocal microscopy image stack, we perform a segmentation that labels each voxel with a cell identifier, forming closed, neighboring 3-dimensional regions

that will constitute the starting point of our mesh generation.

3.1 3-D Cell Segmentation

The method we use to segment the confocal image sequences is based on the MARS pipeline (Fernandez et al., 2010) and uses a seeded 3-dimensional watershed algorithm to extract the regions corresponding to each cell. The accurate identification of cells relies on the determination of seeds, but the method ensures that the regions converge towards each other, without any hole. This guarantees that neighborhood relation between cells and interface surfaces are well defined in every dimension throughout the structure.

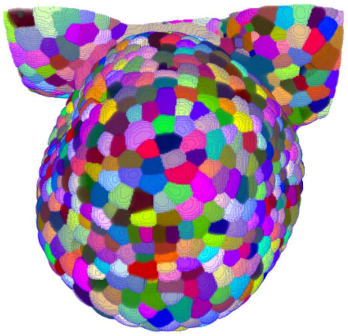

Figure 2: View of the watershed segmentation image obtained on the confocal image stack of a shoot apical meristem.

The resulting segmented images are complex and heavy objects, such as the one depicted in Figure 2. The typical number of regions in the image may reach 3000, each of them containing roughly 20000 voxels. In addition to this excessive weight, the segmented images inevitably present some artifacts leading to noisy boundaries, which could benefit from the smoothing induced by a coarser discrete representation.

3.2 Tetrahedral Mesh Generation

To represent the segmented cells by a mesh structure, our strategy consists in compute the mesh topology using a standard method, and then improve it relatively to the characteristics of our data. Among the various possibilities for generating a mesh topology from the segmented image data, we chose to use a tetrahedral discretization of the whole image domain, based on a Delaunay triangulation refinement algorithm (Shewchuk, 1998). Compared to other methods such as Marching Cubes (Lorensen and Cline, 1987) that generate a huge number of triangles, a triangulation offers the advantage of reducing drastically the volume of information, as it produces from the start a lighter object.

Along with many other computational geometry algorithms, this tetrahedral mesh generation is implemented in the CGAL library (CGAL, 1996), and we used this implementation to generate our mesh topology. The resulting object is a simplicial complex of dimension 3, where each tetrahedron is labeled with a cell identifier.

To convert the simplicial complex into a nested surface mesh, we get rid of the tetrahedra and keep only the triangular faces that are common to two tetrahedra with different labels. Each cell is then bounded by a set of triangles forming a closed surface. Each one of these triangles may be part of (at most) two cells, as the same interface triangle will be assigned to the boundary of the two cells it separates. The resulting mesh constitute an approximation of the complete structure of the tissue, as illustrated in Figure 3.

Figure 3: Surface triangles of the mesh of shoot apical meristem cells built from the tetrahedral mesh generated by Delaunay refinement.

The quality of the image approximation provided by the mesh is controlled in the CGAL implementation by a distance parameter. This value sets the upper bound for the distance between the mesh triangles and the boundaries of their corresponding regions in the image. This parameter has also a strong influence on the complexity of the mesh, as more numerous and smaller triangles are necessary to fit the image boundaries with less error. The optimization performed by lowering this global distance constraint comes with an exponential rise in the number of primitives used to define the surfaces, and consequently does not operate on all the desirable properties of the mesh.

3.3 Quality Criteria

The criteria we would like to see as optimal in the mesh are multiple and not necessarily compatible. The quality objective involves both geometrical and biological factors that should be met with a minimal complexity by the resulting mesh. It is then necessary to define accurately what is a good tissue mesh, and how it is possible to quantitatively evaluate its quality.

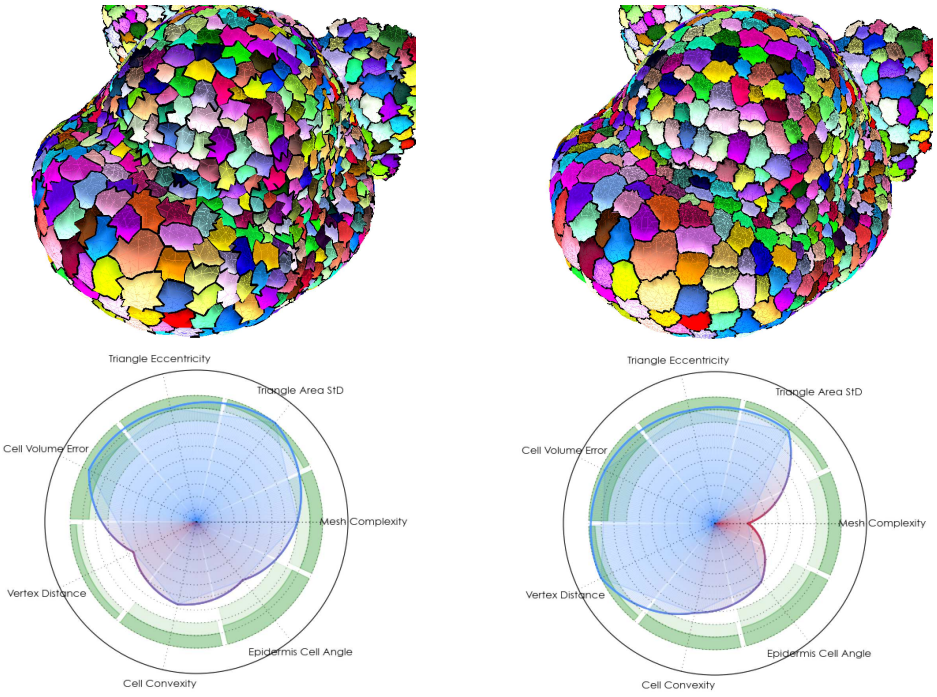

(a) (b)

Figure 4: Comparison of quality criteria measures for two meshes of the same image obtained with distance parameter values of 2.0 voxels (a) and 1.0 voxel (b).

To perform this evaluation, we define **7 quality criteria** that account for the various objectives a cell tissue mesh should fulfill. Those criteria concern the precision with which the mesh fits the input data, the consistency of the shape it defines with those expected from SAM cells, the regularity of the triangles defining the surface, and the number of geometric elements necessary to the representation. A thorough definition of this criteria can be found in Section 5.

Indeed, the reconstructed cells in the final mesh, though consisting of a simplified model, should first correspond as precisely as possible to the cells identified in the original image, and constitute a faithful reconstitution of the segmented voxel image S that can be seen as a ground truth.

- **Region Consistency:** global measure based on the comparison of cell volumes in the mesh and in the original image.
- **Interest Point Preservation:** local measure based on the distance of identified points in the mesh with their matching ones in the image.

A second important aspect is the way the shape of cells in the mesh correspond to the prior knowledge accessible on SAM cells. The resulting mesh must not only coincide with the computer-generated data representing cells, but most importantly to observed cell geometric properties, in order to become a biologically plausible meristem reconstruction and make it possible to draw conclusions from simulations (Figure 5).

- **Cell Convexity:** global measure based on the convexity of the mesh cells, estimated as a volume ratio with their convex hull.
- **Surface Arrangement:** local measure based on the apparent geometry of the surface cells, and the projected angles formed by adjacent cells.

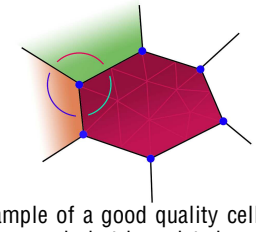

Figure 5: Example of a good quality cell with its interest points : convex, regularly triangulated and with regular angles with neighbors.

The quality of a triangular mesh is more commonly defined by the absence of small or eccentric triangles. Given the goal of using the meshed meristems for physical simulations, the triangles must in any way have properties allowing the application of

finite element methods. Consequently the regularity and homogeneity of the mesh in the shape and size of its surface elements has to be taken into account.

- **Triangle Quality:** global measure based on a triangle eccentricity estimation, measuring how far a given triangle is from an equilateral one.
- **Size Homogeneity:** global measure based on the standard deviation of the areas of triangles to estimate how regular the mesh is.

And finally, a highly desirable property is to reach the aforementioned objectives with as few triangles as possible. In terms of computational cost for visualization and feature extraction, the lighter the mesh is, the better performance will be reached, provided that the other criteria are fulfilled.

- **Mesh Lightness:** global measure based on the number of triangles necessary to represent the surface of a cell.

A simultaneous view of all these quality criteria can be given by a spider chart, as soon as all measurement can be aligned on the same scale (by a normalization between 0 and 1 for instance). This results in a visualization such as those presented in Figure 4 where the overall area of the domain delimited by the values of the different parameters has to be maximal. Any defect in one of the criteria will immediately be reflected in the visualization chart.

Applied to the surface meshes produced by the Delaunay refinement algorithm, such quality estimation highlights the complex optimization problem we are facing. The objective being to maximize all the criteria at the same time, improving the mesh by lowering the distance parameter is not satisfactory, given the drastic loss on the lightness criterion, as it appears strikingly in Figure 4. An acceptable solution should be more of a compromise that tends to optimize all quality criteria for a fixed mesh complexity.

4 MESH OPTIMIZATION

To address the problem emerging from the introduced criteria, we choose to formulate this mesh optimization as an energy minimization problem, in the same spirit as (Hoppe et al., 1993). One objective being to limit the mesh complexity, this task can be performed on a light mesh without any change in its topology, by working only on the mesh geometry.

4.1 Mesh Definitions

The mesh object M we consider is a boundary representation of dimension 3, consisting of four sets of elements W_0, W_1, W_2, W_3 representing respectively vertices, edges, triangles and cells.

The elements themselves are defined by their boundaries in the dimension below, which can be represented by a boundary relationship B_d at dimension d. For instance, an edge $e \in W_1$ is defined by its two vertex extremities $B_1(e) = \{v_1(e); v_2(e)\}; v_1 \neq v_2 \in W_0$, a triangle $t \in W_2$ by its three edges. A cell $c \in W_3$ is the only type of element for which the number of boundary elements (triangles) is not fixed.

The boundary relation can be extended to consider gaps of more than one dimension, for instance to retrieve the vertices of a triangle; this higher dimension boundary relation B_d^n links elements of dimension d with their boundaries at dimension $d - n$, and can be defined recursively : $\forall w \in W_d; B_d^n(w) = \bigcup_{u \in B_d(w)} B_{d-1}^{n-1}(u)$ (with $B_d^1 = B_d$).

This first relationship gives birth to a converse region relationship R_d^n representing, for an element of dimension d, the elements of higher dimension for which it constitutes a boundary:

$$\forall w \in W_d; R_d^n(w) = \{u \in W_{d+n}(M) \mid w \in B_{d+n}^n(u)\}$$

Those two symmetrical relations define two possible neighborhood relations N_d^+ and N_d^- between elements of the same dimension, depending whether we consider that they are connected by a higher dimension region (like two vertices linked by an edge) or by a lower dimension boundary (like two cells sharing an interface triangle):

$$N_d^+(w) = \{w' \in W_d \mid R_d(w) \cap R_d(w') \neq \emptyset\}$$
$$N_d^-(w) = \{w' \in W_d \mid B_d(w) \cap B_d(w') \neq \emptyset\}$$

In addition to this topological aspect, the geometry of the mesh is defined by the association of each vertex $v \in W_0$ with a point in $\mathbb{R}^3$ representing its position $P(v)$ in the image referential. The definition of P determines the shape of every higher dimension element, and plays a predominant part in the quality of the mesh.

Using this representation, our optimization problem comes down to searching optimal positions P of the vertices, an optimization that can be performed without modification of the mesh topology if its initial configuration is satisfactory. Provided an initial mesh $M^{(0)} = \{W_0; P^{(0)}; W_1; B_1; W_2; B_2; W_3; B_3\}$, obtained for instance by Delaunay refinement, the problem is to find the optimal mesh geometry P^t, as the one that minimizes an energy functional accounting for the quality criteria.

4.2 Energy Formulation

Following the widespread approach concerning deformable models, from their first application to con-

tour detection (Kass et al., 1988) to other commonly used models (Chan and Vese, 2001), the energy functional E that we aim at minimizing is defined as a sum of energy terms accounting for the different criteria to be optimized. This general combination applied to 3-dimensional models (Dufour et al., 2011) can be written as:

$$E(M;S) = E_{image}(M;S) + E_{prior}(M) + E_{regularity}(M)$$

There is an identity between the energy terms and the quality criteria we defined. The image, or data attachment, energy should be minimal when the region consistency and interest point preservation criteria are optimal, and the same goes for the prior energy and the cell convexity and surface arrangement criteria, and the internal regularity energy and the triangle quality and homogeneity criteria.

Each one of these three terms is built on local energy potentials defined on the elements of M (and the geometry of their vertices) that estimate the validity of the local configuration regarding the corresponding criterion.

4.2.1 Image Attachment Energy

The surfaces represented by the mesh M are defined to fit the separations between cells in the segmented image S, so that the regions delimiting cells in both representations superimpose as perfectly as possible.

More importance is given to special interest points which are cell corners. These points correspond to those where four cells intersect in S (or three cells at the surface of the tissue) and should particularly be preserved in the mesh for a realistic reconstruction. Such points are very easily accessible in the topology of M as the vertices v for which $R^3_0(v)$ contains four elements (respectively three).

Both the region consistency and the interest point preservation criteria refer to a notion of gradient magnitude in the segmented image S, as separation interfaces are transitions leading to non-zero values of gradient, and cell corners, where many transitions occur, would correspond to local maximal values. However, unlike a color or intensity image, the segmentation S is a label image where the actual values do not matter, only the transitions are to be considered.

Therefore, we approximate the gradient magnitude image $k\nabla Sk$ by considering a spherical neighborhood of radius s around each voxel and count the number of different labels it encloses. To give more weight to exterior object boundaries, the number is doubled when the neighborhood intersects the exterior. This function is then smoothed by a gaussian filter of standard deviation s to obtain a more continuous value.

The energy $E_{gradient}$ associated with this boundary information is defined on the positions P of the vertices of the mesh, and should be minimal when a vertex fits well on a cell interface. We define it simply as the opposite of the gradient magnitude, so that high values of the gradient constitute optimal positions for the vertices of the mesh, weighted by a coefficient $w_{gradient}$:

$$\begin{aligned} E_{image}(M;S) &= \sum_{v \in W_0} w_{gradient} E_{gradient}(v;S) \\ &= \sum_{v \in W_0} w_{gradient} k\nabla S k(P(v)) \end{aligned} \quad (1)$$

4.2.2 Shape Prior Energy

The second energy term gives the possibility of including prior knowledge on the geometry of cells or additional external constraints. The most simple characterization for a SAM cell, and the minimal constraint it should satisfy, is that its surface should form a convex solid with convex planar polygonal facets, such as examples in Figure 6.

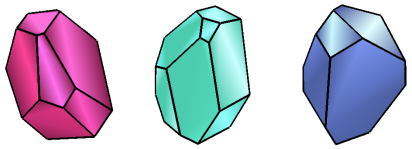

Figure 6: Example of cells as convex solids with planar convex polygonal facets.

From biological expertise, we expect cells to present in most cases planar interfaces, and linear edges that form convex faces, properties that should fulfill the two cell shape criteria. They are translated into two energy potentials defined on the vertices of the mesh:

$$E_{prior}(M) = \sum_{v \in W_0} w_{plan} E_{plan}(v) + w_{line} E_{line}(v) \quad (2)$$

The planarity energy potential $E_{plan}(v)$ simply sums the distances of $P(v)$ to the average planes of all the cell interfaces it belongs to. Those planes are estimated by averaging the normals of the triangles composing the interface, and the distance can be computed as a dot product.

The energy $E_{line}(v)$ is defined on the vertices belonging to at least two cell interfaces, thus part of the contour of a cell interface. To regularize those contours, we chose to sum the laplacian energies of all the interface contours going through v, computed at $P(v)$.

4.2.3 Triangle Regularity Energy

The internal energy term accounts for the regularity of the mesh, and for the optimization of the triangle quality and size homogeneity criteria. This leads to a definition of two energy potentials, this time defined on triangles, but that can commonly be restricted to the vertices of each triangle:

$$E_{regularity}(M) = \sum_{v \in W_0} \frac{1}{3} \sum_{t \in R_0^2(v)} w_{qual} E_{qual}(t) + w_{size} E_{size}(t) \quad (3)$$

It is commonly accepted that a regular triangular surface mesh is composed of vertices of degree 6, connecting 6 even equilateral triangles. The quality energy potential $E_{qual}(t)$ defined on a triangle's geometry $\{P(v), v \in B_2^2(t)\}$ should measure its eccentricity, its deviation from an equilateral configuration. Among the various possible triangle eccentricity measures (Field, 2000), we chose the sum of sinuses, that involves no maximum operator, and has good derivability properties, while being optimal in the equilateral case:

$$E_{qual}(t) = 1 - \frac{2}{3\sqrt{3}} \sum_{v \in B_2^2(t)} \sin\left(P(v)\right) \quad (4)$$

Concerning the size homogeneity potential $E_{size}(t)$, we simply use the squared distance of the triangle area to the average area over all the mesh. Defined this way, this energy is of course minimal when all the triangles have the same size.

4.3 Minimization and Evolution

The minimization of the energy functional E is performed by a local optimization process, based on consecutive small moves of the vertices. The vertex positions P are iteratively updated to decrease the overall value of the energy function, based on decisions made locally on the energy potentials.

To add more control on this operation, at each iteration i, we force the updated position $P^{(i+1)}(v)$ of each vertex to remain within a sphere of radius s_v around its current position $P^{(i)}(v)$. This limitation ensures that the mesh deforms smoothly and limits the risk of fold-overs and intersections between triangles.

The motion of the vertices can be determined by a gradient descent of the local energy potential, following the opposite direction of the local gradient of E, *i.e.* the first order derivative of the energy with respect to P, while staying inside the sphere of radius s_v around $P(v)$:

$$P^{(i+1)}(v) = P^{(i)}(v) - \min\left(1; \frac{s_v}{\left\| \frac{\partial E}{\partial P} \right\|_v}\right) \frac{\partial E}{\partial P}\Big|_v \quad (5)$$

The only exception concerns cell corners, as a matching can directly be performed between those interest points in the mesh and in the image. Their optimal position can therefore be known in advance, and the iterative shifting for the vertices v of M that could be matched to a cell corner in S will simply consist in smoothly traveling along the trajectory between their initial position $P^{(0)}(v)$ and their corresponding image target point $P^{(S)}(v)$.

For the remaining vertices of M, the computation of the functional derivative of the energy can be done using the calculus of variations, and relies on the computation of the derivatives of each term of the overall energy.

4.3.1 Energy Gradient Computation

The formulation of the different energy terms as a sum of local potentials defined on the vertices of the mesh, makes it easy to compute a good approximation of the energy gradient at $P(v)$ as the derivative of the concerned potential in the sum, considering only the vertex v.

The image attachment energy certainly has the simplest formulation regarding this computation, as it is possible to compute the gradient of the approximated gradient magnitude $k-Sk$ in any point of the image. Consequently, the local energy gradient becomes:

$$\frac{\partial E_{gradient}}{\partial P}\Big|_v = -k-Sk(P(v)) \quad (6)$$

Concerning the shape prior energies, the interface planarity potential is a sum of distances to planes. If we consider that the interface planes remain unchanged by shifting one vertex, the derivative of this distance is simply the unitary projective vector of $P(v)$ to the plane, the direction of which is given by the plane's normal. The laplacian formulation of the energy defined for interface contours leads to an easy differentiation. It corresponds to the one involved in the laplacian smoothing operation, where vertices are attracted by the barycenters of their neighbors.

Finally, the gradients of the triangle-based regularity energy potentials, are estimated by considering the derivatives of the potential in one single triangle relatively to the position of one of its vertices. The resulting energy gradient at one vertex is simply obtained by summing the derivatives of the potentials at all neighboring triangles, for instance:

$$\frac{\partial E_{qual}}{\partial P}\Big|_v = \sum_{t \in R_0^2(v)} \frac{1}{3} \frac{\partial E_{qual}(t)}{\partial P}\Big|_v \quad (7)$$

All the triangle energy potentials can be computed using the three lengths of the edges forming the boundary of the triangle, and their derivative can be decomposed over the two lengths l_1 and l_2 involving the considered vertex, as depicted in Figure 7. The decomposition base consists then in two unitary vectors, located in the triangle's plane, and following the direction of the edges, giving the following equation:

$$\frac{\partial E_{qual}(t)}{\partial P}\Big|_v = \frac{\partial E_{qual}(t)}{\partial l_1} \frac{\partial l_1}{\partial P}\Big|_v + \frac{\partial E_{qual}(t)}{\partial l_2} \frac{\partial l_2}{\partial P}\Big|_v \quad (8)$$

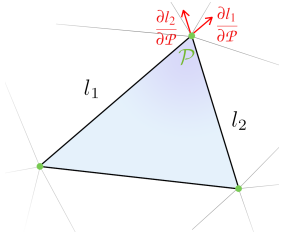

Figure 7: One mesh triangle and the length derivatives used to compute the local energy gradient at point P.

4.3.2 Energy Balancing

As often in energy-based optimization methods, a lot of the algorithm's efficiency relies on the right combination of the weights associated with each energy term to produce a balanced behavior.

In our case, the energies taken separately have very different effects, with almost contradictory results. For instance, considered alone, the image energy will push the mesh vertices towards the local maxima of the approximated gradient $k-Sk$ in a converging way : all the vertices in the neighborhood of one maximum will be attracted by it. This generates small and possibly irregular triangles as it is visible in Figure 8 (a), in complete contradiction with the regularity energy.

The same goes for planarity and linearity energies, as projections on a plane for example might create flat triangles depending on its original orientation, as in Figure 8 (b). The regularization energy will then generally have an antagonist effect on the behavior of the other forces. It acts as a rigidity constraint trying to preserve the good properties of the mesh triangles, through the global displacement induced by the remaining energies.

Acting alone however, it fails to produce realistic cell shapes, leading to noisy edges and irregular cell

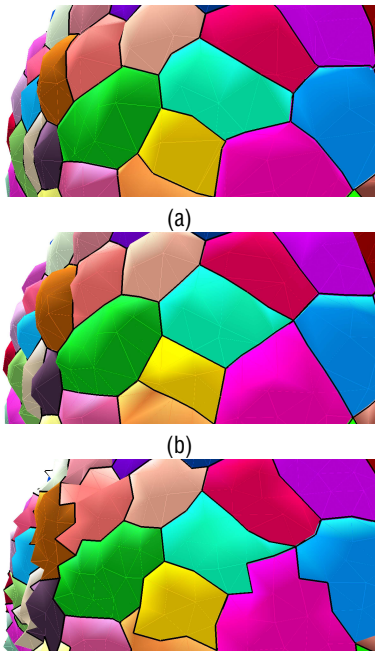

(a) (b) (c)

Figure 8: Effects of the optimization of the different energy terms on the mesh : image energy (a) shape prior energy (b) and regularity energy (c).

facets (as the shape of triangles is optimizes without regard on the consequences on the surface geometry). This is clear on the very regular mesh of Figure 8 (c) where almost equilateral triangles generate very irregular borders.

It is then very important to balance it well relatively to the shape an image terms to have an evolution where the influence of the latter is visible (the rigidity of the mesh should not prevent him from deforming) while the regularity of the triangles is preserved (and not crushed by the destructive effects of the other energies).

To find the weights offering the best compromise between the intrinsic quality of the mesh and the its consistency with the data, we used the 7 quality criteria our process is implicitly designed to maximize. By exploring the value space for the set of parameters w, and calculating the correlation of the quality estimators with the different values, we estimated a best joint configuration of the energy weights:

- $w_{gradient} = 0.17$
- $w_{qual} = 2.0$
- $w_{plan} = 0.47$
- $w_{size} = 0.005$
- $w_{line} = 1.3$
- $s_v = 1.0$

4.3.3 Optimization Results

We applied our mesh optimization method to tissue meshes of different shoot apical meristems obtained form the Delaunay tetrahedral mesh generation. The cell corners are optimized with their extracted image position, and the rest of the mesh vertices by energy gradient descent.

The termination criterion is set to be a fixed number of iterations rather than a measure of deformation between two iterations. One of the reasons for this choice is that the energy minimum for the data attachment energy would be a mesh where vertices concentrate at local gradient maxima. Though the regularization energy works against this tendency, it is not guaranteed to find a globally stable configuration avoiding this problem, and it was sensible to stop the evolution as soon as the energies have all had the time to play their role, with 20 iterations.

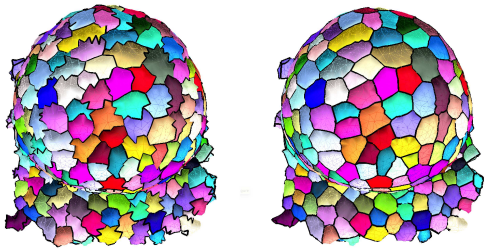

Figure 9: Example of the application of our optimization process on a meristem mesh.

The result of the optimization is a mesh with the same topology as the initial one, but with a geometry that makes it much more consistent with the cell regions in the image and with their biological reality at the same time. This better consistency visible in Figure 9 is achieved without any unnecessary complication of the mesh, which keeps a constant number of elements all along the process.

4.4 Implementation Details

The algorithms detailed above were implemented in Python 2.7, using the standard NumPy and SciPy libraries, and wrappers for the C++ CGAL library.

An implementation constraint comes from the fact that 16-bit labels are not handled by CGAL the mesh generation function. Consequently, the processing of images with more that 255 cells requires a re-labeling step before the mesh generation, and the re-affectation of original labels to the connected components in the resulting tetrahedral complex.

Concerning execution times, the complexity proves to be linear with respect to the number of cells in the image, as the number of triangles varies proportionally with it. The typical computation times for a 2000 cell image is of 125s for the mesh generation and 130s for its optimization, provided the costly filtering of the image necessary for the gradient and the cell corner extraction (depending on the image size) has been computed beforehand.

5 EVALUATION

To assess the quality of the reconstructed tissue meshes, we generated meshes over several segmented SAM images, and computed the estimators for the seven quality criteria. We give here a formal definition of these normalized estimators, using the notations of our mesh representation:

- **Region Consistency** (optimized by E_{image}) computed using the average volume error, $V_M(c)$ representing the volume of cell c in the mesh and $V_S(c)$ in the image:

$$q_{region} = 1 - \frac{1}{|W_3|} \sum_{c \in W_3} \frac{|V_M(c) - V_S(c)|}{V_S(c)}$$

- **Interest Point Preservation** (optimized by E_{image} and by cell corner extraction) computed using the average minimal distance of a cell corner P' in the image to a cell corner of the mesh, normalized by the maximal 26-neighborhood distance:

$$q_{point} = \min\left(1; \frac{\sqrt{3}}{\frac{1}{|Corners_S|} \sum_{Corners_S} \min_{Corner_M(v)} (\|P(v) - P'\|)}\right)$$

- **Cell Convexity** (optimized by E_{prior}) computed using the average ratio between the volume $V_M(c)$ of the cell c and the volume of the convex hull H of its vertices:

$$q_{convexity} = \frac{1}{|W_3|} \sum_{c \in W_3} \frac{V_M(c)}{V(H(\bigcup_{v \in B_3^3(c)} P(v)))}$$

- **Surface Arrangement** (implicitly optimized) computed using the average squared deviation of projected cell angles on the tangent plane at surface cell corners $q_v(c)$ to $\frac{2\pi}{3}$, corresponding to a regular configuration:

$$q_{angle} = \min\left(1; \frac{\pi}{2} \sqrt{\frac{1}{p=3} \frac{1}{|Corner_M|} \sum_{Corner_M(v)} \frac{1}{|R_0^3(v)|} \sum_{c \in R_0^3(v)} (q_v(c) - \frac{2\pi}{3})^2}\right)$$

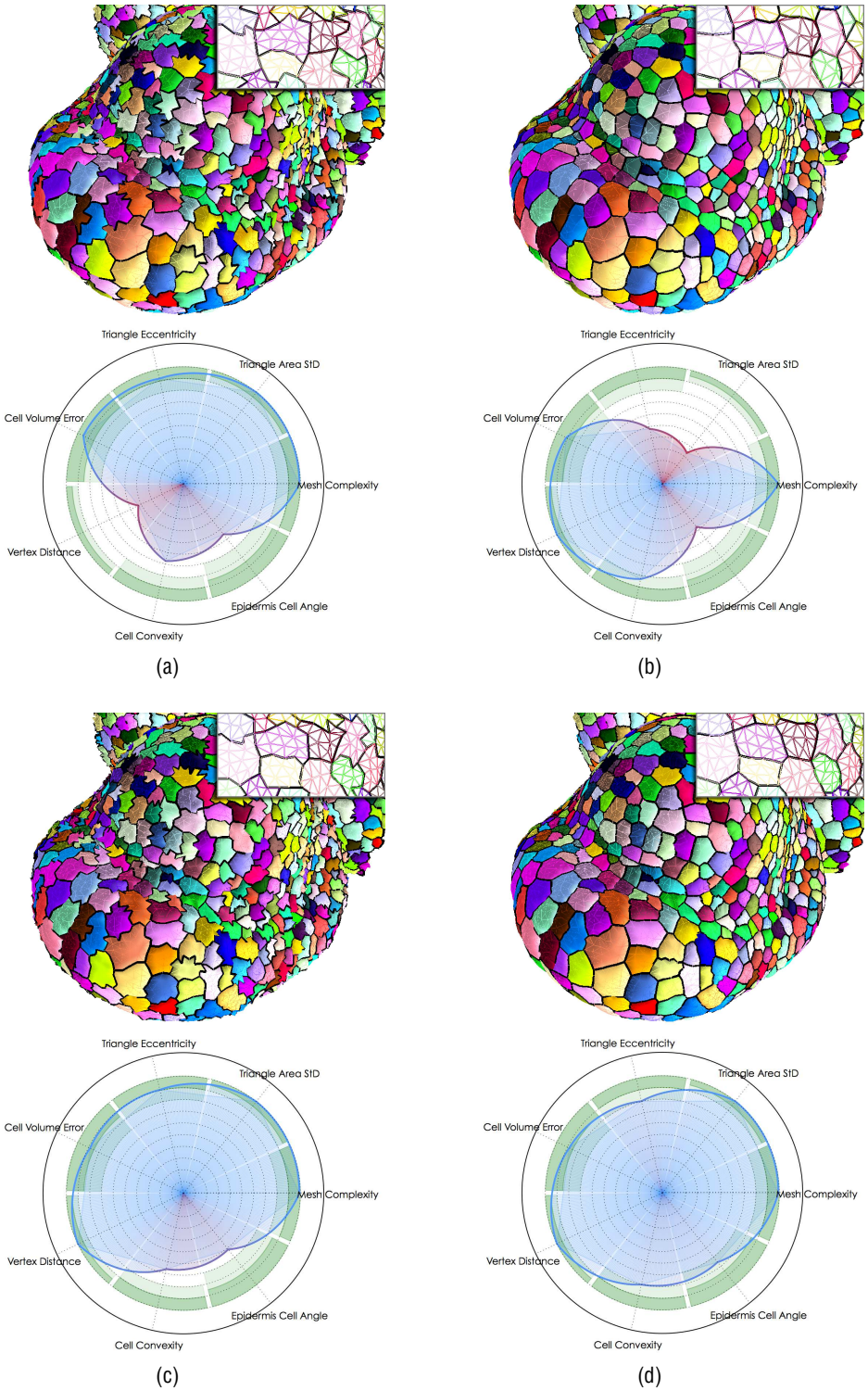

Figure 10: Validation of the SAM mesh optimization results through the comparison of average mesh quality estimators on original meshes (a) and on the corresponding optimized meshes using image attachment energy only (b), using regularity energy only (c) and with the full energy (d).

- **Triangle Quality** (optimized by $E_{regularity}$) computed using the average eccentricity of all the mesh triangles, estimated using the sum of sinuses:

$$q_{triangle} = \frac{1}{|W_2|} \sum_{t \in W_2} \frac{2}{3\sqrt{3}} \sum_{v \in B_2^2(t)} \sin P(v)$$

- **Size Homogeneity** (optimized by $E_{regularity}$) computed using the standard deviation of the areas A of all the mesh triangles, normalized by their average area $\bar{A}$:

$$q_{homogeneity} = \min\left(1; \frac{\sqrt{\frac{1}{|W_2|} \sum_{t \in W_2} (A(t) - \bar{A})^2}}{\frac{1}{|W_2|} \sum_{t \in W_2} A(t)}\right)$$

- **Mesh Lightness** (optimized by the distance parameter of the mesh generation) computed using the average number of triangle necessary to represent one cell, normalized by the number $n_{oct} = 152$ obtained for a good triangulation of a space-filling truncated octahedron:

$$q_{lightness} = \min\left(1; \frac{n_{oct}}{\frac{1}{card(W_3)} \sum_{c \in W_3} \mathrm{card}(B_3(c))}\right)$$

(an empirical value of $\sqrt[3]{\frac{1}{3\sqrt{3}}} \sqrt{\frac{1}{|W_3|} \sum_{c \in W_3} V_S(c)}$ for the distance parameter proved to give values of $q_{lightness}$ between 0.95 and 1)

Such an evaluation framework opens the way to a rather exhaustive quantification of the quality of a SAM tissue mesh, both from an intrinsic point of view and from the comparison with real-life data. Based on their typical values on reference quality meshes, we associated each quality estimator with acceptability thresholds, represented as green ranges on the diagrams. As such, it constitutes an original tool to assess whether a mesh representing a complex plant cell tissue satisfies all the necessary computational and visual properties.

This evaluation framework is also flexible as it can be adapted to different types of *a priori* constraints in the definition of the quality criteria, for instance if one deals with other types of tissues. In such a case, it is possible to select and quantify additional criteria for mesh quality and integrate them in the energy functional as well as on the evaluation spider representation.

Applied to both the initial meshes and the resulting optimized meshes, this evaluation method underlines the contribution of our optimization process. The results, averaged over several images containing 1000 to 3000 cells, are presented in Figure 10. To analyze the results with more precision, we compared the quality estimators from the initial meshes (Figure 10 (a)), with those achieved by different variants of the energy:

- **Image attachment Energy** (Figure 10 (b)): the minimization of E_{image} only leads to a valuable improvement of cell shapes while providing an excellent approximation of the image data. However the geometry of the mesh triangles is destroyed, which is clearly visible in the performance over regularity criteria. The apparition of degenerated triangles penalizes this scores and gives locally wrong configurations, around cell corners notably.
- **Regularity Energy** (Figure 10 (c)): the optimization based on the minimization of $E_{regularity}$ (along with the optimal cell corner shifting) appears as an effective way of preserving, if not improving, the overall quality of the mesh triangles, throughout the deformation induced by the motion of the vertices. Still, the visual impression produced by this optimization appears very poor, which is confirmed by the mitigated performance reached on the cell shape quality criteria.
- **Full Energy** (Figure 10 (d)): it appears then clearly that the addition of the other energy terms is essential to obtain a globally satisfying result. The quantitative measures show that regularization forces and shape/image forces have antagonist effects, the latter tending to improve the cell shape related criteria with a strong counterpart on the triangle quality criteria. Their simultaneous application constitutes an improvement on both sides, as the rigidity provided by the regularity term compensates the natural tendency of the other terms to flatten the triangles, while leaving enough flexibility to allow for both objectively and visually satisfactory cell reconstructions.

The optimization through the balanced combination of the different energies appears then as the only way to obtain an overall optimal compromise that does not neglect any aspect of the quality criteria. The result is a mesh that models in a visually convincing way the shape and disposition of the cells in the meristem, with a high regularity of the triangles, and a strong consistency with the original image, while preserving an overall complexity low enough to make it exploitable for visualization and simulation uses.

6 CONCLUSIONS

The method we presented to reconstruct a complex triangular mesh of a shoot apical meristem cell tis-

sue actually bridges a gap between experimental data, and higher-level computational simulations. The mesh representation we obtain constitutes a ready-to-process object, including local shape information as well as tissue-scale topological relations. It opens the way to a great deal of potential applications, from fast shape feature extraction using discrete geometry, to statistical computations (average shapes, extended to average tissue) or physical and mechanical growth simulations. Using growing real-world examples rather than hand-built model structures would constitute a major step for the validation of such biophysical development models.

All of this of course holds only if the provided reconstruction presents the properties needed to make these applications possible and sensible. Our optimization process guarantees that the produced mesh reconstructs faithfully the experimental data, with a complexity that will make processing times reasonable, and by geometrical elements regular enough to expect correct simulations. The quantitative quality evaluation framework we designed ensures that the compromise between these hardly consonant aspects fulfills the necessary criteria. It additionally provides an objective and complete measure of the quality of a SAM tissue mesh, that could be used to compare different methods.

A further improvement in mesh quality could be reached by optimizing simultaneously the mesh topology along with its geometry, and perform operations of vertex insertion and suppression based on the same energy minimization process. Such an approach would allow to dynamically improve the local topology (that now may still lead to noisy cell edges) and optimize the mesh lightness along with the other quality criteria.

The performance reached by the mesh optimization method we described is already enough to consider that the step of converting an image in a higher-level representation is crossed, and the ensuing applications in computation and simulation at reach. It constitutes in any way an additional tool of great interest for the better understanding of plant morphogenesis.

REFERENCES

Amenta, N., Bern, M. W., and Eppstein, D. (1997). Optimal point placement for mesh smoothing. In *Proceedings of the ACM-SIAM Symposium on Discrete Algorithms*, pages 528–537.

Barbier de Reuille, P., Bohn-Courseau, I., Godin, C., and Traas, J. (2005). A protocol to analyse cellular dynamics during plant development. *The Plant Journal*, 44(6):1045–1053.

Barbier de Reuille, P., Robinson, S., and Smith, R. S. (2014). Quantifying cell shape and gene expression in the shoot apical meristem using MorphoGraphX. In *Plant Cell Morphogenesis*, pages 121–134.

Chakraborty, A., Perales, M. M., Reddy, G. V., and Roy Chowdhury, A. K. (2013). Adaptive geometric tessellation for 3d reconstruction of anisotropically developing cells in multilayer tissues from sparse volumetric microscopy images. *PLoS One*, 8(8).

Chakraborty, A., Yadav, R., Reddy, G. V., and Roy Chowdhury, A. K. (2011). Cell resolution 3d reconstruction of developing multilayer tissues from sparsely sampled volumetric microscopy images. In *BIBM*, pages 378–383.

Chan, T. and Vese, L. (2001). Active contours without edges. *IEEE Transactions on Image Processing*, 10(2):266–277.

Dufour, A., Thibeaux, R., Labruyere, E., Guillen, N., and Olivo-Marin, J.-C. (2011). 3-d active meshes: Fast discrete deformable models for cell tracking in 3-d time-lapse microscopy. *IEEE Transactions on Image Processing*, 20(7).

Fernandez, R., Das, P., Mirabet, V., Moscardi, E., Traas, J., Verdeil, J.-L., Malandain, G., and Godin, C. (2010). Imaging plant growth in 4D : robust tissue reconstruction and lineaging at cell resolution. *Nature Methods*, (7):547–553.

Field, D. A. (1988). Laplacian smoothing and delaunay triangulations. *Communications in Applied Numerical Methods*, 4(6):709–712.

Field, D. A. (2000). Qualitative measures for initial meshes. *International Journal for Numerical Methods in Engineering*, 47(4):887–906.

Freitag, L. A. (1997). On combining laplacian and optimization-based mesh smoothing techniques. In *Trends in Unstructured Mesh Generation*, pages 37–43.

Guignard, L., Godin, C., Fiuza, U.-M., Hufnagel, L., Lemaire, P., and Malandain, G. (2014). Spatio-temporal registration of embryo images. In *IEEE International Symposium on Biomedical Imaging*.

Hoppe, H., DeRose, T., Duchamp, T., McDonald, J., and Stuetzle, W. (1993). Mesh optimization. In *Proceedings of the 20th Annual Conference on Computer Graphics and Interactive Techniques*, SIGGRAPH '93, pages 19–26.

Kass, M., Witkin, A., and Terzopoulos, D. (1988). Snakes: Active contour models. *International Journal of Computer Vision*, 1(4):321–331.

Keller, P. J. (2013). Imaging morphogenesis: Technological advances and biological insights. *Science*, 340(6137).

Kwiatkowska, D. (2004). Surface growth at the reproductive shoot apex of Arabidopsis thaliana pin-formed 1 and wild type. *Journal of Experimental Botany*, 55(399):1021–1032.

Lorensen, W. E. and Cline, H. E. (1987). Marching cubes: A high resolution 3d surface construction algorithm. In *Proceedings of the 14th Annual Conference on*

Computer Graphics and Interactive Techniques, SIGGRAPH '87, pages 163–169.

Michelin, G., Guignard, L., Fiuza, U.-M., Malandain, G., et al. (2014). Embryo cell membranes reconstruction by tensor voting. In *IEEE International Symposium on Biomedical Imaging*.

Owen, S. J. (1998). A survey of unstructured mesh generation technology. In *International Meshing Roundtable*, pages 239–267.

Rizzi, B. and Peyrieras, N. (2014). Towards 3d in silico modeling of the sea urchin embryonic development. *Journal of Chemical Biology*, 7(1):17–28.

Robin, F. B., Dauga, D., Tassy, O., Sobral, D., Daian, F., and Lemaire, P. (2011). Time-lapse imaging of live Phallusia embryos for creating 3d digital replicas. *Cold Spring Harbor Protocols*, 1244(6).

Shewchuk, J. R. (1998). Tetrahedral mesh generation by Delaunay refinement. In *Proceedings of the Fourteenth Annual Symposium on Computational Geometry*, SCG '98, pages 86–95.

Tataw, O. M., Reddy, G. V., Keogh, E. J., and Roy Chowdhury, A. K. (2013). Quantitative analysis of live-cell growth at the shoot apex of arabidopsis thaliana: Algorithms for feature measurement and temporal alignment. *IEEE/ACM Trans. Comput. Biology Bioinform.*, 10(5):1150–1161.

CGAL (1996). CGAL, Computational Geometry Algorithms Library. http://www.cgal.org.

Vidal, V., Wolf, C., and Dupont, F. (2012). Combinatorial mesh optimization. *The Visual Computer*, 28(5):511–525.